Topology Optimization Using Gabor Filter: Application to Synchronous Reluctance Motor

Yoshitsugu Otomo[1,2], and Hajime Igarashi[1], *Member, IEEE*

[1]Graduate School of Information Science and Technology, Hokkaido University, Sapporo 060-0814, Japan
[2]Research Fellow of Japan Society for the Promotion of Science (JSPS), Tokyo 102-0083, Japan

This paper proposes a novel topology optimization method using the Gabor filter, which is widely used in the field of image processing. The proposed method is applied to the optimization of a synchronous reluctance motor; its average torque is maximized, and simultaneously, the torque ripple is minimized. It is shown that the proposed method results in a motor with thin layer-shaped flux barriers, which achieves a better torque performance in comparison with a conventional model and a motor optimized using NGnet.

***Index Terms*—Gabor filter, Genetic algorithm (GA), Synchronous reluctance motor (SynRM), Topology optimization.**

I. Introduction

The synchronous reluctance motor (SynRM) has been widely used in various electric apparatuses because of its low manufacturing cost and simple structure. To improve the performance of SynRM, parameter optimization of flux barriers in the rotor core has been performed [1]–[3]. This approach can improve the motor performance but can make it difficult to obtain new rotor shapes.

Topology optimization, which will be discussed in this paper, allows us to obtain a novel motor structure with excellent performance. In particular, the on/off method based on the normalized Gaussian network (NGnet) has been shown to be effective for the design of electric motors such as permanent magnet motors [4, 5] and SynRMs [6]. However, when using this method, it is difficult to obtain thin-layered flux barriers that effectively generate the reluctance torque for SynRMs and other rotating machines. This is due to the fact that optimization tends to converge to the rotor shape with thick or large flux barriers because they are robust against the fluctuation in material distribution; thus, the objective function has a rather broad distribution in the search space. In contrast, thin-layered flux barriers can easily be broken by perturbation in material distribution. This implies that a small change in material distribution can have a significant impact on the magnetic field distribution in the rotor. Hence, the corresponding objective function may be steep, making it difficult for optimization algorithms to find the optimum. Indeed, this tendency can be observed when the gradient-based method is employed [7, 8].

This study aimed to develop a topology optimization method through which high-performance solutions can be obtained including structures with thin-layered flux barriers. In this paper, we propose a novel topology optimization method using the Gabor filter, which is widely used in image processing [9]. The proposed method will make it possible to represent thin flux barriers because the Gabor filter can represent spatial anisotropy. Moreover, because our approach can apply a real-coded genetic algorithm (GA), global search can be performed without relying on the initial shape, unlike gradient-based methods. The proposed method is applied to the topology optimization of an SynRM, aiming at the maximization of the average torque and minimization of the torque ripple. The performance of the SynRM optimized using the proposed method is compared with that of a conventional SynRM with thin flux barriers and a motor optimized using the NGnet method.

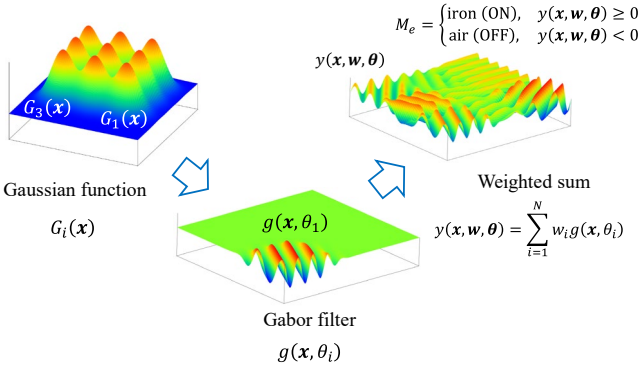

Fig. 1. On/off method using Gabor filter

II. Optimization Method

Topology optimization using the Gabor filter is schematically shown in Fig. 1. The material distribution in the design region Ω_{core} is determined from the value of the shape function defined by

$$y(\boldsymbol{x},\boldsymbol{w},\boldsymbol{\theta}) = \sum_{i=1}^{N} w_i g(\boldsymbol{x},\theta_i) \tag{1}$$

where w_i $(-1 \leq w_i \leq 1)$ and N denote the weighting coefficient and the number of the Gabor filters, respectively. The function $g(\boldsymbol{x},\theta_i)$ in (1) is the Gabor filter defined by

$$g(\boldsymbol{x},\theta_i) = b_i(\boldsymbol{x}) \cos[k(X_i \cos\theta_i + Y_i \sin\theta_i)] \tag{2}$$

Manuscript received November 26, 2020 and accepted February 2, 2021.
Corresponding author: Y. Otomo (e-mail: otomo@em.ist.hokudai.ac.jp)
Color versions of one or more of the figures in this paper are available online at http://ieeexplore.ieee.org.
Digital Object Identifier (inserted by IEEE).

where k, $(X_i, Y_i) = (x - x_i, \quad y - y_i)$, $\boldsymbol{x}_i \equiv (x_i, y_i)$, and θ_i $(0 \le \theta_i \le 2\pi)$ denote the wavenumber, position vector of the Gabor filter, center of Gaussian basis $G_i(\boldsymbol{x})$, and rotation angle, respectively. Moreover, $b_i(\boldsymbol{x})$ is the normalized Gaussian function, which is given by

$$b_i(\boldsymbol{x}) = G_i(\boldsymbol{x}) \Big/ \sum_{j=1}^{N} G_j(\boldsymbol{x}) \tag{3}$$

$$G_i(\boldsymbol{x}) = \frac{1}{(2\pi)\sigma^2} \exp\left\{-\frac{1}{2\sigma^2}|\boldsymbol{x} - \boldsymbol{x}_i|^2\right\} \tag{4}$$

where σ and $\boldsymbol{x}$ denote the standard deviation and position vector, respectively. The material attribute M_e of finite element e in Ω_{core} is determined as

$$M_e = \begin{cases} \text{iron (ON)}, & y(\boldsymbol{x}, \boldsymbol{w}, \boldsymbol{\theta}) \ge 0 \\ \text{air (OFF)}, & y(\boldsymbol{x}, \boldsymbol{w}, \boldsymbol{\theta}) < 0 \end{cases} \tag{5}$$

It is observed that the topology optimization is now reduced to parameter optimization with respect to $\boldsymbol{w} = [w_1, w_2, \ldots, w_N]^{\mathrm{t}}$ and $\boldsymbol{\theta} = [\theta_1, \theta_2, \ldots, \theta_N]^{\mathrm{t}}$, where N denotes the number of unknowns in each variable. In the optimization process, $\boldsymbol{w}$ and $\boldsymbol{\theta}$ are determined so as to minimize the objective function $F(\boldsymbol{w}, \boldsymbol{\theta})$ that will be given below by a real-coded genetic algorithm (GA), called AREX+JGG [10], which shows the good performance in ill-conditioned and variable dependent problems.

III. Optimization of SynRM

A. Optimization Problem

The rotor shape of the reference model, which has three flux barriers per pole, is shown in Fig. 2. In addition, TABLE I summarizes the model parameters and driving conditions. The purpose of the optimization is to maximize the average torque T_{ave} while minimizing the torque ripple T_{rip}. Thus, we solve the optimization problem defined by

$$\min_{\boldsymbol{w},\boldsymbol{\theta}} F(\boldsymbol{w}, \boldsymbol{\theta}), \quad F(\boldsymbol{w}, \boldsymbol{\theta}) = -\frac{T_{\text{ave}}(\boldsymbol{w}, \boldsymbol{\theta})}{T_{\text{ref1}}} + \alpha \frac{T_{\text{rip}}(\boldsymbol{w}, \boldsymbol{\theta})}{T_{\text{ref2}}} \tag{6}$$

where $T_{\text{ave}}(\boldsymbol{w}, \boldsymbol{\theta})$, $T_{\text{rip}}(\boldsymbol{w}, \boldsymbol{\theta})$, T_{ref1}, and T_{ref2} denote the average torque and torque ripple for the optimized and reference models, respectively. Moreover, α is the weighting coefficient that controls the balance between the first and second term. In this work, we set $\alpha = 0.25$.

We optimize the rotor colored in green shown in Fig. 3. Topology optimization is performed only for the half rotor region Ω_{core} assuming mirror symmetry. Considering manufacturing, the surfaces of the rotor core facing the shaft and air gap are excluded from the design region.

B. Optimization Setting

In this topology optimization, $30N$ individuals were generated for the first generation, and $8N$ children were generated from $2N + 1$ parents at each generation. The evolution process was continued over 1,500 generations in the abovementioned setting. It took approximately 6 days to obtain the optimization results using an Intel Xeon CPU (3.5 GHz, 16 threads).

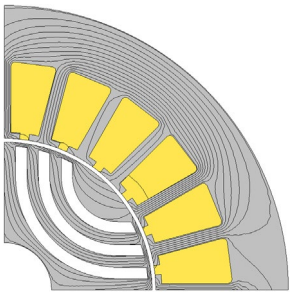

Fig. 2. Reference model ($T_{\text{ave}} = 0.96$ Nm, $T_{\text{rip}} = 22.4$ %)

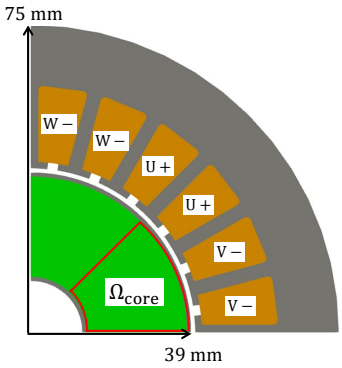

Fig. 3. Optimization is performed for Ω_{core} considering mirror symmetry.

TABLE I
SPECIFICATIONS OF REFERENCE SYNRM

Phase and pole	Three-phase, four poles
Coil current (A)	3.0
Driving frequency (Hz)	20
Initial current phase angle (deg)	135
Number of coil turns	100
Rotation speed (r/min)	600
Thickness (mm)	37.5
Rotor and stator grade	50JN400

IV. Optimization Results

A. Optimization Using Gabor Filter and NGnet

To validate the performance of the proposed topology optimization using the Gabor filter, (6) is also solved using the NGnet-based on/off method [4], where if the wavenumber $k = 0$ in (2), the Gabor filter corresponds to NGnet.

We uniformly deploy the basis functions for the proposed method and the NGnet method as shown in Fig. 4. The design region is covered by the circular domain of influence of the basis functions centered at $\boldsymbol{x}_i$. To compare the two optimization methods using the same number of unknowns, $2N$ Gaussian bases are deployed in the design region for NGnet as shown in Fig. 4 (b) because the design variables in the Gabor filter are $2N$. The resultant rotor shapes are shown in Fig. 5 where the

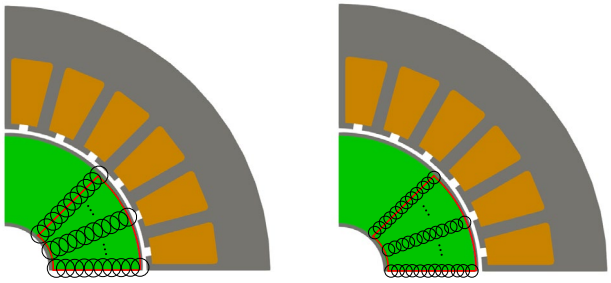

(a) Gabor filter
($\sigma = 3.0$ mm, $\lambda = 6.0$ mm $N = 78$)

(b) NGnet
($\sigma = 2.0$ mm, $N = 156$)

Fig. 4. Distribution of each basis

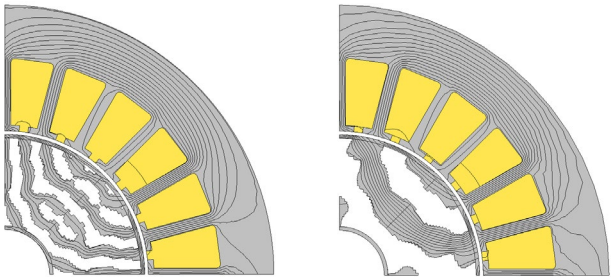

(a) (b)

Fig. 5. Resultant rotor shapes. (a) Gabor filter ($T_{\mathrm{ave}} = 0.97$ Nm, $T_{\mathrm{rip}} = 9.6$ %). (b) NGnet ($T_{\mathrm{ave}} = 0.92$ Nm, $T_{\mathrm{rip}} = 24.2$ %).

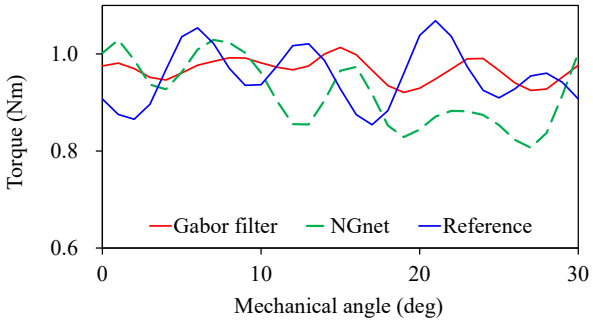

Fig. 6. Torque waves for resultant shapes

values of the average torque and torque ripple are described. We can see that the rotor shape obtained by the Gabor filter shown in Fig. 5 (a) has thin flux barriers along the *d*-axis in a way similar to that of the reference model in Fig. 2. In contrast, the rotor obtained by NGnet shown in Fig. 5 (b) consists of thick flux barriers despite of the fine distribution of the Gaussian basis functions. Similar thick flux barriers have been obtained in conventional works [6]–[8].

The torque waves for the reference and optimized shapes are shown in Fig. 6. The torque ripple for Fig. 5 (a) is considerably smaller than that of the reference model, while there is no significant difference in the average torque. The NGnet method can moderately improve the average torque and torque ripple. The dominant Fourier components of the torque and magnetic force density for the optimized and reference rotor shapes are shown in Fig. 7 to clarify the difference between the torque ripples for these rotor shapes. The magnetic force density $T_{\mathrm{r}\theta}$ in the air gap in Fig. 7 (b) is computed from the Maxwell stress tensor as follows:

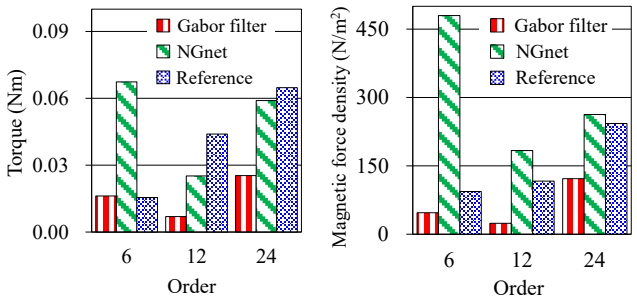

(a) Torque (b) Magnetic force density

Fig. 7. Spectrum of torque and magnetic force density

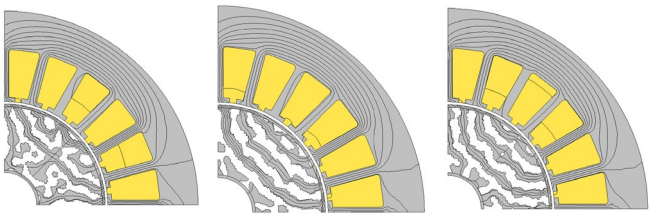

(a) (b) (c)

Fig. 8. Resultant rotor shapes at each generation optimized by Gabor filter (a) 200 generation ($T_{\mathrm{ave}} = 0.82$ Nm, $T_{\mathrm{rip}} = 19.0$ %), (b) 500 generation ($T_{\mathrm{ave}} = 0.90$ Nm, $T_{\mathrm{rip}} = 14.0$ %), (c) 550 generation ($T_{\mathrm{ave}} = 0.91$ Nm, $T_{\mathrm{rip}} = 12.1$ %)

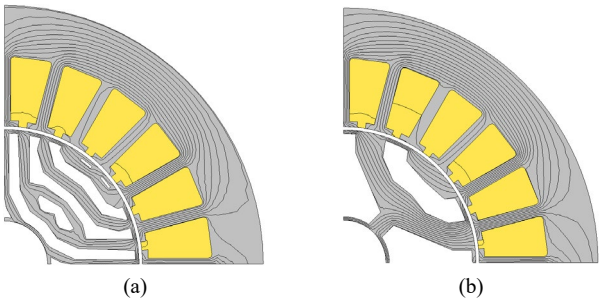

(a) (b)

Fig. 9. Smoothed rotor shapes. (a) Gabor filter ($T_{\mathrm{ave}} = 1.0$ Nm, $T_{\mathrm{rip}} = 9.9$ %). (b) NGnet ($T_{\mathrm{ave}} = 0.82$ Nm, $T_{\mathrm{rip}} = 35.4$ %)

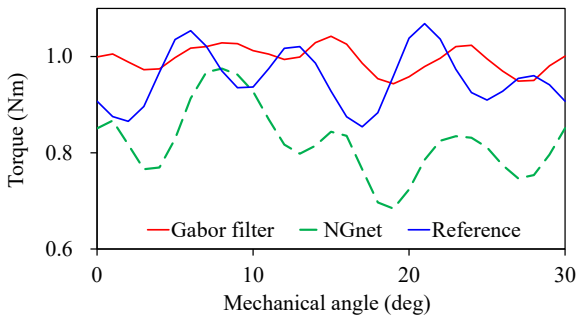

Fig. 10. Torque waves for smoothed rotor shapes

$$T_{\mathrm{r}\theta} = \frac{1}{2\mu_0} B_{\mathrm{r}} B_{\theta} \tag{7}$$

where μ_0, B_{r}, and B_{θ} denote the vacuum permeability, radial and circumferential magnetic flux densities, respectively. Fig. 7 (a) shows that the rotor shape shown in Fig. 5 (a) effectively decreases the 12th and 24th order harmonics, which generate the torque ripple. The higher harmonics in the magnetic energy are

also reduced in the motor shown in Fig. 5 (a). The motors in Fig. 2 and Fig. 5 (b) have relatively large harmonics both in terms of the torque and magnetic energy.

The best rotor shapes at 200th, 500th, and 550th generations optimized using the Gabor filter are shown in Fig. 8. There are minor changes in the average torque after the 500th generation, while there are slow but continuous changes in the torque ripple until the final generation. We do not observe significant changes in the rotor shape after the 500th generation. This suggests that the torque ripple is very sensitive to the core structure. The final rotor shape shown in Fig. 5(a) is obtained after a delicate tuning of the structure of the rotor core.

B. Smoothing of Rotor Shapes for Manufacturing

Although the optimized rotor shapes shown in Fig. 5(a) and Fig. 5(b) are relatively simple, the rotor surfaces are wavy. In terms of manufacturing, it may be better to make these shapes smoother. The smoothed rotor shapes and their torque waves are shown in Figs. 9 and 10. We can see that the simplification of Fig. 5(a) has no significant effect on the performance as shown in Figs. 9(a) and 10. In contrast, as the main magnetic flux changes by connecting the rotor core to the shaft, the performance shown in Fig. 9(b) is significantly deteriorated. This result indicates the superiority of the Gabor filter at least for the optimization of SynRMs.

C. Discussion for Gabor Filter Setting

It is suggested that the resultant solution obtained by the Gabor filter depends on the wavelength and the number of deployed Gabor filters. To clarify the difference between the optimization results, we consider cases with a different wavelength λ and a different density of the Gabor filter shown in Fig. 11, where λ is smaller than the tooth width of the stator core in (a) while the filter is made to be coarser in (b). The resultant rotor shapes are shown in Fig. 12. The optimized shape shown in Fig. 12(a) is rather complicated and its average torque is less than that for Fig. 5(a). In contrast, the resultant shape shown in Fig. 12(b) achieves almost the same performance as the motor in Fig. 5(a). Further reduction in the number of the Gabor filters would deteriorate the representation of the thin-layered structures.

V. Conclusion

In this paper, we have proposed a novel topology optimization method for SynRMs using the Gabor filter. It has been shown that the optimized SynRM using the Gabor filter has thin-layered flux barriers with good performance both in terms of average torque and torque ripple. The proposed method is concluded to be suitable for the optimization of SynRMs. The wavelength of the Gabor filter should be set to be larger than the tooth width. The proposed method can be applied to the topology optimization of rotor and stator shapes of permanent magnet motors, which will be discussed in future studies.

Acknowledgment

This work was supported in part by the JSPS KAKENHI Grant Number JP19J20375 and in part by the MEXT Doctoral program for the Data-Related InnoVation Expert Hokkaido University (D-DRIVE-HU) Program.

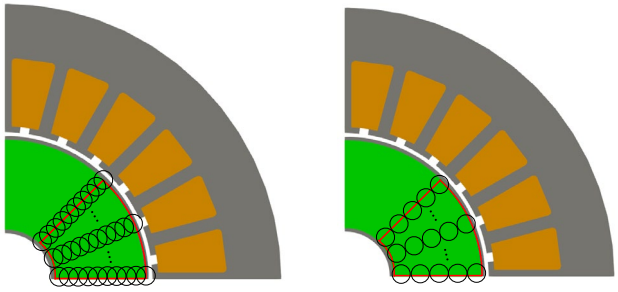

(a) (b)

Fig. 11. Distribution of Gabor filters. (a) $\sigma = 3.0$ mm, $\lambda = 3.0$ mm, $N = 78$. (b) $\sigma = 3.0$ mm, $\lambda = 6.0$ mm, $N = 22$.

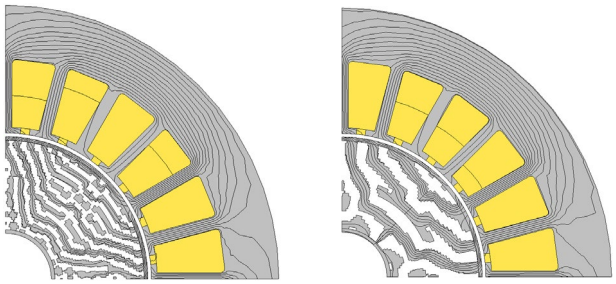

(a) (b)

Fig. 12. Resultant rotor shapes obtained by different settings for Gabor filter. (a) $T_{\text{ave}} = 0.85$ Nm, $T_{\text{rip}} = 13.0$ %. (b) $T_{\text{ave}} = 0.95$ Nm, $T_{\text{rip}} = 12.1$ %.

References

[1] F. Cupertino, G. Pellegrino, and C. Gerada, "Design of Synchronous Reluctance Motors with Multiobjective Optimization Algorithms," *IEEE Trans. Ind. Appl.*, vol. 50, no. 6, pp. 3617-3627, 2014.

[2] Y. Wang, D. M. Ionel, V. Rallabandi, M. Jiang, and S. J. Stretz, "Large-Scale Optimization of Synchronous Reluctance Machines Using CE-FEA and Differential Evolution," *IEEE Trans. Ind. Appl.*, vol. 52, no. 6, pp. 4699-4709, 2016.

[3] M. H. Mohammadi, R. C. P. Silva, and D. A. Lowther, "Incorporating Control Strategies into the Optimization of Synchronous AC Machines: A Comparison of Methodologies," *IEEE Trans. Magn.*, vol. 54, no. 3, Art. no. 8101204, 2018.

[4] T. Sato, K. Watanabe, and H. Igarashi, "Multimaterial Topology Optimization of Electric Machines Based on Normalized Gaussian Network," *IEEE Trans. Magn.*, vol. 51, no. 3, Art. no. 7202604, 2015.

[5] H. Sasaki, and H. Igarashi, "Topology Optimization Accelerated by Deep Learning," *IEEE Trans. Magn.*, vol. 55, no. 6, Art. no. 7401305, 2019.

[6] S. Sato, T. Sato, and H. Igarashi, "Topology Optimization of Synchronous Reluctance Motor Using Normalized Gaussian Network," *IEEE Trans. Magn.*, vol. 51, no. 3, Art. no. 8200904, 2015.

[7] Y. Okamoto, R. Hoshino, S. Wakao, and T. Tsuburaya, "Improvement of Torque Characteristics for a Synchronous Reluctance Motor Using MMA-based Topology Optimization Method," *IEEE Trans. Magn.*, vol. 54, no. 3, Art. no. 7203104, 2018.

[8] Y. Yamashita and Y. Okamoto, "Design Optimization of Synchronous Reluctance Motor for Reducing Iron Loss and Improving Torque Characteristics Using Topology Optimization Based on Level-set Method," *IEEE Trans. Magn.*, vol. 56, no. 3, Art. no. 7510704, 2020.

[9] J. R. Movellan, "Tutorial on Gabor Filters," MPLab Tutorials, Univ. California, San Diego, USA, Tech. Rep., 2005.

[10] A. Komori, Y. Maki, M. Nakatsui, I. Ono, and M. Okamoto, "Efficient Numerical Optimization Algorithm Based on New Real-Coded Genetic Algorithm, AREX+JGG, and Application to the Inverse Problem in Systems Biology," *Applied Mathematics*, vol. 3, no. 10, pp. 1463-1470, 2012.